Proceedings of IDETC/DTM 2011
ASME 2011 International Design Engineering Technical Conferences &
Computers and Information in Engineering Conference
August 29-31, 2011, Washington, DC, USA

DETC2011-48619

A TWO DEGREE OF FREEDOM NANOPOSITIONER WITH ELECTROTHERMAL ACTUATOR FOR DECOUPLED MOTION

Yong-Sik Kim
Intelligent Systems Division, National Institute of Standards and Technology,
100 Bureau Drive, Gaithersburg, MD 20899, USA

Nicholas G. Dagalakis
Intelligent Systems Division, National Institute of Standards and Technology,
100 Bureau Drive, Gaithersburg, MD 20899, USA

Satyandra K. Gupta
Department of Mechanical Engineering
and Institute for Systems Research
University of Maryland
College Park, Maryland 20742, USA

ABSTRACT

Building a two degree-of-freedom (2 DOF) Micro Electro Mechanical Systems (MEMS) nanopositioner with decoupled X-Y motion has been a challenge in nanopositioner design. In this paper a novel design concept on making the decoupled motion of the MEMS nanopositioner is suggested. The suggested nanopositioner has two electrothermal actuators and employs a fully nested motion platform with suspended anchors. The suggested MEMS nanopositioner is capable of delivering displacement from the electrothermal actuator to the motion platform without coupled motion between the two X-Y axes. The design concept, finite element analysis (FEA) results, fabrication procedures, and the performance of the 2 DOF nanopositioner are presented. In order to test the nanopositioner moving platform decoupled motion, one actuator moves the platform by 60 μm, while the other actuator is kept at the same position. The platform position cross talk error was measured to be less than 1 μm standard deviation.

1 INTRODUCTION

Two Degree of Freedom (DOF) nanopositioners have been used in a variety of applications requiring micro precision positioning mechanisms like optical fiber alignment [1], micromanipulation [2, 3, 19], and material property testing [4]. Nanopositioners based on microelectromechanical systems (MEMS) fabrication are also attractive due to their low costs, batch process, and small size, which make MEMS nanopositioners flexible for system integration. Nanopositioners must have the capability of actuating the nanopositioner large displacements along two independent axes. An understanding of the kinematics of the 2 DOF nanopositioner will enable modeling of the nanopositioner and improve the control of the actuators.

A typical two DOF MEMS nanopositioner design is a simple combination of two or more single DOF actuators to generate the required 2 DOF motions. Due to limitations in MEMS fabrication, some systems generate motions along independent axes coupled to each other. Once the motion generated by the actuators is coupled or inevitably linked to the structure, the non-linear kinematic model is needed to resolve the final output or displacement [5]. Thus, the coupled multi-DOF nanopositioning structures discussed above need an elaborate kinematic analysis to predict and control its behavior [13].

An alternative way is to design all actuation structures along independent axes that are mechanically decoupled. With decoupled actuation structures, no interference or coupling effects are expected between the actuation systems. In this case, the kinematic model becomes simple and easy to use by aligning the actuation direction along the axis [2]. Hence, the decoupled system is proposed in this paper.

The actuator in the nanopositioner is a transducer to transform the electric energy into mechanical form. The mechanical form is displacement for the moving platform. Various actuators, like electrostatic [6], electromagnetic [7], and electrothermal [8, 9] actuators, have been adopted to actuate nanopositioners. Among these three candidates, the ability to generate enough force required by the design concept is important in the selection of the actuator, since the nanopositioner is supposed to have external mechanical loads. An example of the mechanical loads is manipulating samples for an atomic force microscope. Also the stiffness of the designed structure has to be considered in designing a nanopositioner and the stiffer structure requires higher actuation force. Therefore the bent-beam type electrothermal actuator is a promising candidate for a nanopositioning system.

The electrothermal actuator is known for its capability to generate a larger force than electromagnetic or electrostatic actuators [8, 10]; the force generated by the electrothermal actuator is up to tens of milli-Newton, while the electromagnetic or electrostatic actuator can generate up to hundreds of micro-Newton. This is one reason why electrothermal actuators are popular for building and assembling three dimensional space (3D) structures that require large force [20]. We have experience in using the three different types of actuators for our nanopositioners. The nanopositioner described in this paper has about 40 N/m to 50 N/m of electrothermal actuator stiffness [2, 18] and can move up to 50 um in displacement. Based on our experience, the electrothermal actuator is the best choice for the actuator type where high levels of stiffness and force are needed.

With the electrothermal actuator, the structure holding both ends of its beam plays an important role in its performance. If both ends of the electrothermal actuator are firmly fixed, all generated force is transformed to displacement. Otherwise, a portion of the force will be dissipated in deforming the holding structure, which is very undesirable. In general, this is not a serious problem in single DOF actuation. Unlike 1 DOF actuators, 2 DOF actuators have a higher possibility to have some problem related to their supporting structure. The supporting structures which hold both ends of the electrothermal actuator are generally located outside the moving platform. In this case, if there is need to actuate an inner platform, an outer actuation structure can be used. A solution to this problem is to use a compliant coupling mechanism for designing 2 DOF nanopositioners [2].

In a partially nested structure, one moving platform, the so called inner platform, is surrounded by the other moving platform, called the outer platform, but its actuator is external. The supporting frame outside the outer platform is utilized as the platform base for this actuator. The design of the mechanical connection from this actuator to the inner platform becomes important. It is difficult to fabricate traditional universal joint or 3D link mechanisms using MEMS fabrication methods, unless the limited compliant mechanism are used. Our previous design [2] utilized a double parallelogram flexure, shown in Figure 1. This flexure is supposed to transfer fully actuated force to the moving platform and absorb (or minimize) cross-coupling motion.

However, this compliant mechanism is neither perfectly stiff along the actuation axis nor perfectly flexible along the orthogonal axis. The ANSYS[1] Finite Element Model (FEM) structural analysis shows its intrinsic problems; the compliant mechanism coupling of the inner platform works as additional stiffness for the external nanopositioner axis according to the Finite Element Analysis (FEA) results shown in Figure 2(a). The FEA results in Figure 2(a) show the expected displacement analysis when the outer actuation is active while the inner actuation is not. The electrothermal actuator for the outer platform is externally actuated to move 10 um in this FEA model and thus the outer platform is expected to move 100 um due to the 1:10 ratio lever mechanism in the design. But because of the compliant mechanism, the maximum displacement in the outer platform is expected to be 32.207 um from Figure 2(a). This means that only 32 % of the force from the electrothermal actuator transfers to the outer platform because of imperfectness of the compliant mechanism. In addition, the asymmetry layout caused by this compliant mechanism makes itself operate as a pivot for the outer platform, so unexpected rotational motion up to 20 um around the compliant mechanism is noticeable as shown in Figure 2(b). To eliminate those unexpected motions, the elimination of the compliant mechanism is necessary. A new mechanism that has a fully nested structure with released anchors is being proposed in this research.

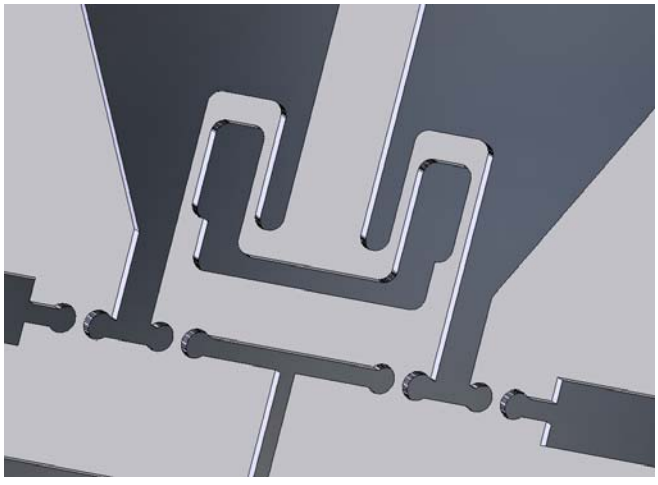

Figure 1. Prior design that used a double parallelogram flexure [2]

[1] Certain commercial equipment is identified in this paper to adequately describe the experimental procedure. Such identification does not imply recommendation or endorsement by the National Institute of Standards and Technology nor does it imply that the equipment identified is necessarily the best available for the purpose.

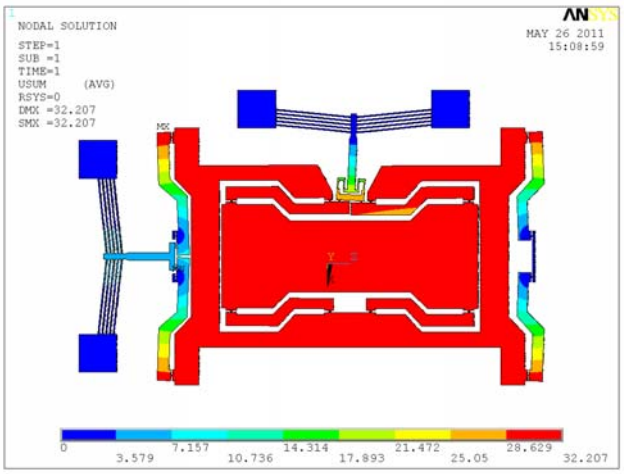

(a) FEA displacement results for prior design (in μm unit)

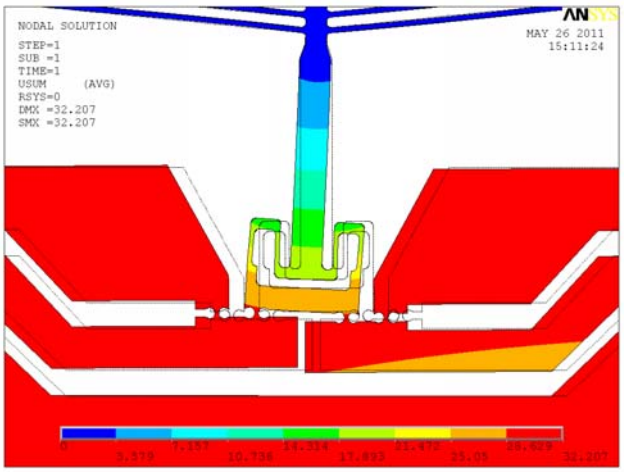

(b) Undesirable rotation around flexure was observed with the prior design (in μm unit)

Figure 2. Analysis of coupling motion for the design shown in Figure 1

In this paper, a novel fully nested 2 DOF nanopositioner platform has been designed and fabricated. This fully nested design avoids any use of a coupled compliant mechanism, thus this mechanism can minimize coupled motion error along the independent axes. It can also guarantee the displacement equivalent to that of a 1 DOF nanopositioner. For this fully nested structure, an additional structure is required to hold the inner and outer platforms; the released anchors and structure are added onto the backside of the inner platform to hold the electrothermal actuator in the inner platform and the inner platform itself. Several prototypes were fabricated and tested with a Veeco Optical Profiler and a JEOL Scanning Electron Microscope (SEM).

2 DESIGN AND ANALYSIS

The basic schematic drawing of the fully nested structure is shown in Figure 3, describing the actuators, the inner and outer platforms, and motion-amplifying levers. The outer platform is surrounded by flexure 2, 3, 4, 5, 6, 7, 8, and 9. The inner platform is surrounded by flexure 12, 13, 14, 15, 16, 17, and 18. The motion-amplifying levers used in this system are combinations of flexure 1, 2, and 3 and 8, 9, 10 for the outer platform and combinations of flexure 11, 12, and 13 and 18, 19, and 20 for the inner platform.

The inner platform, including an electrothermal actuator and four levers, is fully surrounded by the outer platform through flexures from 11 to 20. Because of the fully nested structure design, it does have the limitations from the complex compliant mechanism discussed earlier. The older double parallelogram flexure design had severely coupled motion and poor performance that should be avoided.

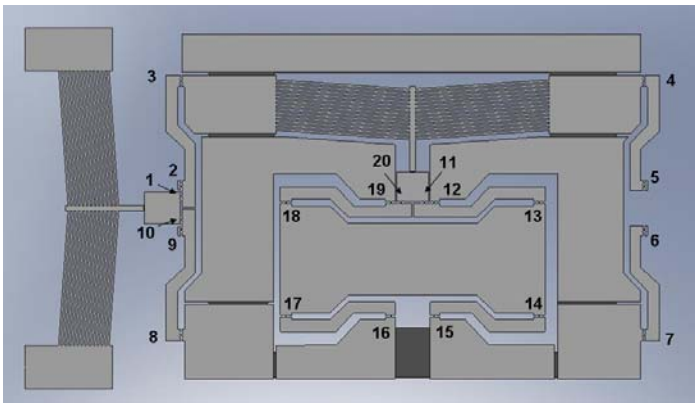

Figure 3. A novel fully nested design of a 2 DOF nanopositioner

The electric power connection for the actuator of the inner moving platform is through metal connections deposited on structures from the outer metal pad, located on the supporting frame, through flexure 2, then flexure 3, to the inner electrothermal actuator. The circuit then closes through flexure 4, to flexure 5, and finally the other outer metal pad. To avoid any current leakage, trenches are etched between adjacent flexures; flexure 1 and the outer electrothermal actuator, flexure 11 and the inner electrothermal actuator, flexure 12 and the inner electrothermal actuator, flexure 5 and 7, and flexure 6 and 8. These trenches are etched on the silicon on insulation (SOI) device layer (top conducting silicon crystal layer), but still maintain connectivity through the supporting SOI silicon lower layer (bottom silicon layer). These two layers of silicon are separated by an insulating thin layer of silicon dioxide.

The outer platform has a horse-shoe shape with an opening between flexures 15 and 16 as shown in Figure 3. This opening is for the inner platform to move. The outer platform also supports the whole inner platform through flexures 3, 4, 7, and 8. Due to the suspended anchors beneath the outer platform and inner platform, the whole system keeps its shape during operation.

The design process of the proposed 2 DOF nanopositioning system is composed of two parts; 1) modification of the electrothermal actuators utilized for both inner and outer platforms and 2) design of fully nested 2 DOF nanopositioner platform. Based on previous electrothermal actuator research work [1, 2, 9], the modification process starts with the assumption that there is the external mechanical load to move, and the actuator should generate both enough displacement and force for the external platform to move. The calculated range of motion of the platform with the modified electrothermal actuator is about 60 μm to 70 μm.

2.1 Design of the electrothermal actuator

Figure 4 shows a schematic drawing of the electrothermal actuator. The stiffness of the electrothermal actuator can be expressed as [8]:

$$K_{actuator} = \frac{2\sin^2(\theta)WTE}{L} \quad (1)$$

where E is the Young's modulus of the material, W is the width of the actuator beams, L is the beam length, T is the thickness of the beam, and θ is the tilt angle of the beam.

The stiffness of the moving platform is a combination of the stiffness of the compliant mechanism flexures. The stiffness of the circular flexures utilized for this analysis can be expressed as [11]:

$$K_{flexure} \approx \frac{2ET}{9\pi}\sqrt{\frac{b^5}{R}} \quad (2)$$

where R is the radius of curvature and b is the width of the flexure.

Therefore, the total stiffness of the moving platform is:

$$K_{stage} = mK_{flexure} \quad (3)$$

where m is the coefficient representing the number of flexures and the geometric layout including the lever mechanism.

With (1) and (3), the total stiffness of the system including the actuator and the moving platform is determined.

$$\frac{1}{K_{total}} = \frac{1}{K_{platform}} + \frac{1}{K_{actuator}} \quad (4)$$

The main factor that determines the maximum range of motion is the buckling load of the electrothermal actuator bent-beam. All long rod structures under longitudinal load will experience buckling if the external load is over the buckling limit [12]. After buckling occurs, the bent-beam in the electrothermal actuator no longer generates force. Therefore, the design that maximizes the buckling load of the bent-beam can increase the displacement of the platform.

The maximum buckling load for the bent-beam can be determined based on the bent-beam geometry. The maximum thrust force from the electrothermal actuator shown in Figure 4 can be expressed as:

$$F_{thrust} = 2nP_{buckling}\sin\theta \quad (5)$$

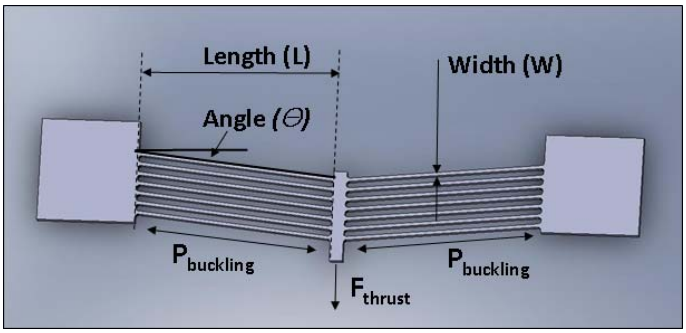

Figure 4. Design of electrothermal actuator with notation used to describe bent-beam design

where $P_{buckling}$ is the maximum buckling load the single beam can hold, θ is the tilt angle, and n is the number of the bent-beams.

Where $P_{buckling}$ can be expressed as [12]:

$$P_{buckling} = \frac{k\pi^2 EI}{L_c^2} \approx \frac{\pi^2 EI}{L^2} \quad (6)$$

where I is the area moment of inertia, L is the length of the bent-beam, and E is the Young's modulus of silicon.

The critical length for buckling load (L_c) is the same with the length of the bent-beam. This is because the boundary of the bent-beam can be regarded as a fixed-guided condition [13].

So, the thrust force can be expressed as:

$$F_{thrust} \approx 2n\frac{\pi^2 EI}{L^2}\sin\theta \qquad (7)$$

Based on the maximum force in equation (7) and the total stiffness of the system in equation (4), the expected displacement can be obtained:

$$F_{thrust} = K_{total}U \qquad (8)$$

The U in the equation (8) represents the displacement at the point between the electrothermal actuator and the outer platform.

Based on the equation (1), (7), (8), and the original dimensions in reference [2], the reasonable dimension range of three design parameters are chosen and listed in Table 1.

Design parameter	Range
Width of beam (W)	10 to 16 μm
Angle of the bent-beam (θ)	0.09 to 0.11 rad
Length of beam (L)	800 to 1200 μm

Table 1. The dimensional range of design parameters

Based on data in Table 1, the sensitivity analysis, 2^k factorial design is exploited. The 2^k factorial design is good at evaluating impact of each design parameter and the joint effect between design factors [21]. For 2^k factorial design analysis, the 10-step analysis software is utilized, which is available to the public provided by NIST Statistical Engineering Division [22, 23]. In the 2^3 factorial design, *θ, L, W* are selected and have two levels with "+" and "-" notation as listed in Table 2. A total of eight different combinations are possible for three design parameters.

Design parameter	-		+
Width of beam (W) (μm)	10	14	16
Angle of the bent-beam (θ) (rad)	0.09	0.1	0.11
Length of beam (L) (μm)	800	1000	1200

Table 2. 2^3 factorial design for design of the electrothermal actuator

Eight different electrothermal actuator designs are made based on combinations of design parameters and utilized in ANSYS[1] FEA simulations. The obtained FEA data for eight different designs are exploited in the 10-step analysis software to check sensitivity of each design parameter. The final regress model from the software can be expressed as;

$$Displacement = 4.658L+3.484W+1.055L*W+1.001\theta*L -0.608\theta*W-0.405\theta-0.143\theta*L*W \qquad (9)$$

From the above regression model, the coefficients of each factor are related to their effect on the performance. The effect of beam length (L) is 4.658, which is 25 % higher than the effect of beam width (W). From this analysis, beam length is more critical than beam width in given design parameters. The third main factor is interaction effect between beam length (L) and beam width (W). From this analysis, the beam length (L) and beam width (W) should be superior to other factors. In addition, the design goal is to make beam length (L) longer and beam width (W) wider for better performance. But beam angle (θ) is not a critical factor, so θ is determined after beam length (L) and beam width (W) are fixed. Table 3 shows the final determined dimensions for each design parameter.

Design parameter	Final value
Width of beam (W)	16 μm
Angle of the bent-beam (θ)	0.1 rad
Length of beam (L)	1200 μm

Table 3. Selected actuator design dimensions

With these selected dimensions, the largest displacement of the platform is expected to be around 70 μm based on FEA results.

2.2 Design of the 2 DOF nanopositioner

The 2 DOF nanopositioner proposed in this paper is a combination of two single DOF platforms for 2 DOF motion that has a fully nested structure with suspended anchors. This design is used in order to minimize coupled motion. Due to the suspended anchors, the fully nested structure can be realized for the inner platform. To utilize this anchored structure beneath the inner platform, the dual layer structure is introduced; the main layer is called the device layer and is utilized for major components and the other layer is called a supporting layer utilized for anchors to hold the structures in the device layer in position. Based on these new features, the 2 DOF nanopositioner is designed as shown in Figure 5(a) and 5(b). Except for four squares indicated by arrows (a), most structures shown in Figure 5(a) are made on the device layer by Deep Reative Ion Etcher (DRIE). The four square structures indicated by arrows (a) and in yellow color are made by metal deposition for the electric connection. The thick dark grey structures indicated by arrows (b) in Figure 5(b) are made at the handle layer with DRIE.

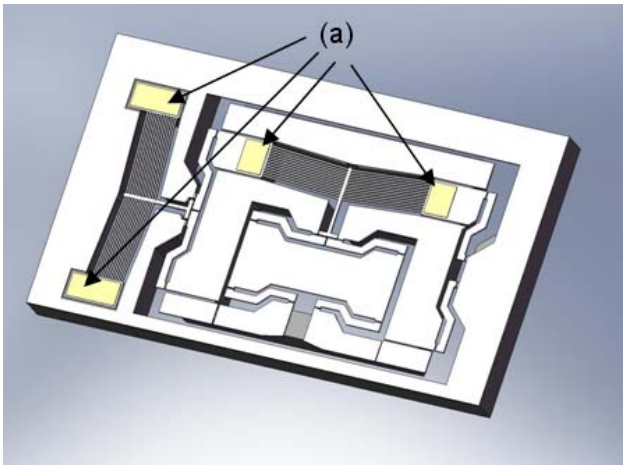

(a) Front side view

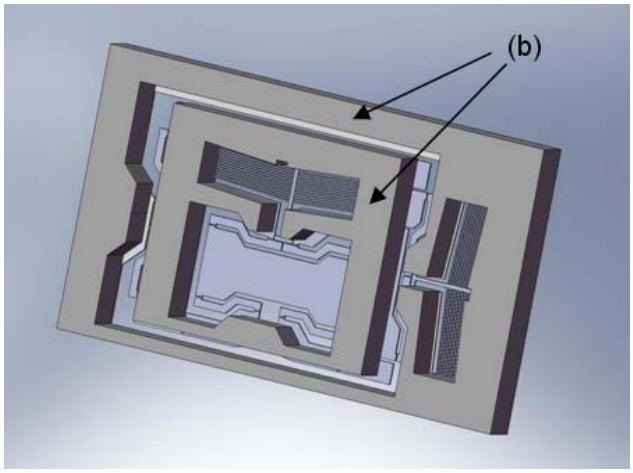

(b) Back side view

Figure 5. 3D Model for the schematic drawing shown in Figure 3

The front side design is shown in Figure 5(a). A single DOF platform consists of an actuator, four levers, and a moving platform. The moving outer platform includes the whole inner platform for 2 DOF motion. Several trenches between the electrothermal actuators and levers are also shown in Figure 5(a). These are used for electric isolation between the two actuators to avoid any electric coupling. The metal pads for the outer platform are next to the actuator, but the metal pads for the inner platform are connected to the inner actuator through long wires, which starts from the pad outside the outer platform to the actuator in the inner platform through flexures and levers in-between. Therefore, the total resistance of the inner actuator is two or three times greater than the resistance of the outer actuator. The real resistance of the actuator in the inner platform after fabrication was found to be 350 Ω, while in the outer platform the resistance was 90 Ω.

The suspended anchors are shown in Figure 5(b). The structures surrounding the bent-beam type electrothermal actuator are anchors designed to hold the actuator in position. To avoid any tilting from unbalanced weight, the center of mass of the supporting structure is located in the center line of the outer platform.

In order to fabricate the two actuators and the suspended anchors, SOI wafers composed of three layers were selected. The device layer (top side of SOI wafer) was used for the main structures and the handle layer (back side of SOI wafer) was utilized as supporting structure for the features on the top side. All nanopositioners were designed based on the popular SOI wafers fabrication recipe known as the SOIMUMPs process [14].

2.3 Finite Elements Analysis (FEA) of the 2 DOF nanopositioner

The FEA is utilized for modeling the mechanical behavior of the suggested design to verify the validity of the analytic expression (8). The electrical, thermal, and structural analyses are combined together in FEA. Multiphysics coupled field simulation was selected as the analysis option. The FEA environment used to perform the analysis is ANSYS[1] ver. 11 [15] on Microsoft Windows XP[1] 64 bit with 16 GB memory computer. In this FEA, the temperature distribution results are obtained from the electrical-thermal analysis and these results are utilized for the thermal expansion calculation of the bent-beam in the structural analysis to obtain the displacement of the moving platform.

The material properties of silicon used for the FEA are described in Table 4 (temperature T is in°C). The resistivity of silicon was calculated based on the measured resistance value for temperatures ranging from 20 ℃ to 55 ℃ and the cross sectional area and length of bent-beam.

Young's modulus (GPa)	169
Poisson's ratio	0.23
Resistivity (Ω μm)	$2.75T - 8x10^{-11}$
Coefficient of thermal expansion (C.T.E.) (1/℃)	$5x10^{-15}T^3 - 1x10^{-11}T^2 + 7x10^{-9}T + 2x10^{-6}$
Thermal conductivity (pW/(μm℃))	$-0.01183T^3 + 296.18T^2 - 266172T + 1x10^8$
Melting point (℃)	1410
Yield strength (GPa)	7

Table 4. Material properties of silicon

The actuation for this FEA was accomplished by applying electrical potential differences, 5V, between two ends of the electrothermal actuator. For the inner platform actuation, the electric connection is achieved by applying 5 V on flexure 2.

Flexure 5 is grounded. For the outer platform actuation, the electric connection is done by directly applying voltage on the pad adjacent to the electrothermal actuator. For the thermal analysis, the temperature at both ends of the electrothermal actuators are set as room temperature, 25℃. Convection and radiation are ignored in this analysis.

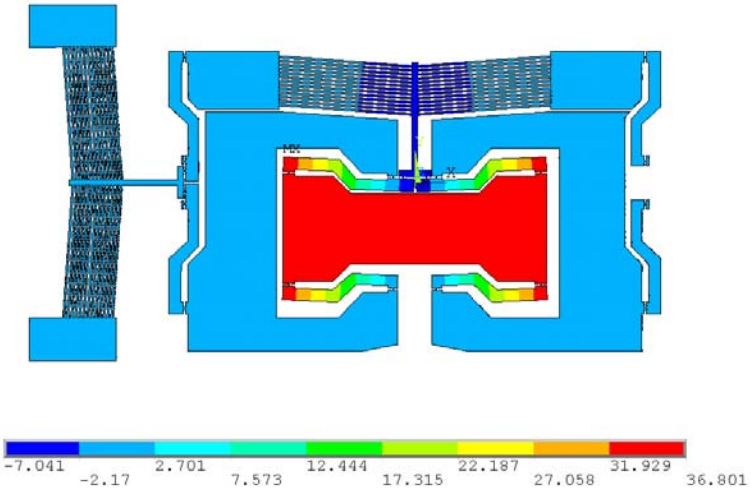

(a) FEA displacement results for new nested design (in μm unit)

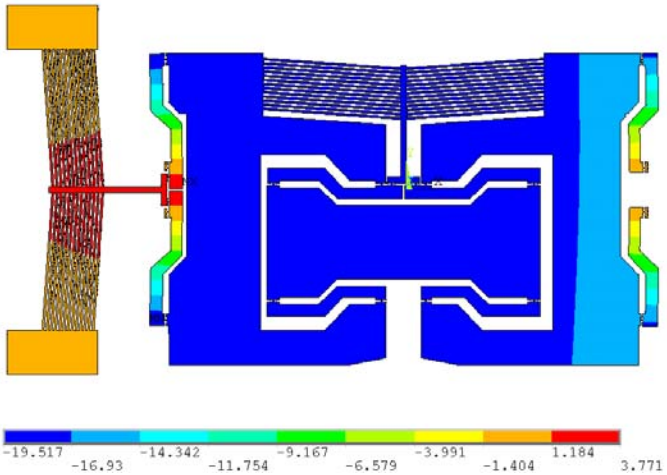

(b) FEA displacement result of the outer platform for new nested design (in μm unit)

Figure 6. ANSYS simulation results for the new nested design shown in Figure 5

With this actuation voltage, the inner platform is actuated up to 36 μm, as shown in Figure 6(a). There is no noticeable coupling or unexpected motion between the two moving platforms in this result. The outer platform is also actuated by the same amount of voltage and the result is in Figure 6(b). The expected displacement by this voltage is about 19 μm and no coupled motion is noticeable in this simulation. Due to different electric connection paths causing different total resistance, the displacement results along the independent axes are not the same.

3 FABRICATION

The 2 DOF nanopositioner requires large displacement and a robust structure. All structures are fabricated on a relatively thick silicon wafer with bulk micromachining. Instead of depositing an additional layer for the supporting structure, the backside or handle layer of the Silicon on Insulator (SOI) wafer is utilized for convenience. A SOI wafer with in-plane diameter of 100 mm is used. The wafer is composed of a topside 30 μm thickness single crystal silicon layer (upper thin grey part in Figure 7(a)), 2 μm thickness buried oxide layer (pink thin strip in Figure 7(a)), and 400 μm thickness backside silicon layer (lower thick grey part in Figure 7(a)). The topside layer is boron-doped to keep resistivity less than 0.2 ohm-cm which allows the electrothermal actuators to operate for up to 20 V actuation voltages. The top and bottom side of the SOI wafer are polished for lithography work on both sides.

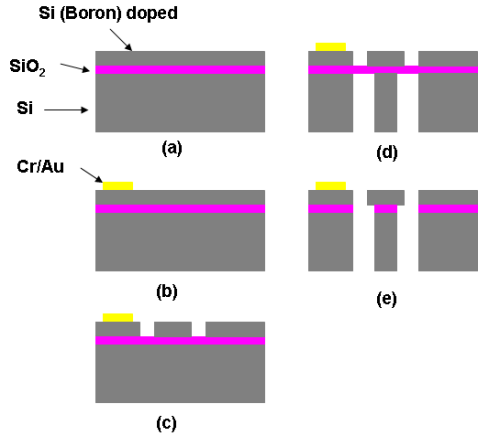

Figure 7. Fabrication sequence for SOI wafer for 2D actuation structure

The first process in the fabrication is the deposition of the metal pads, which are connected to the electrothermal actuator and used for external electric connection through wire bonding. A metal stack of 10 nm of chrome and 50 nm of gold is deposited by an electron-beam evaporator and patterned through a lift-off process using Lift-Off Resists (LOR)-5A and SPR220-3 photoresists (Figure 7(b)). After the lift-off process, the top side is patterned lithographically and deep reactive ion etched down to the buried oxide layer (Figure 7(c)). With these processes completed, the fabrication of all the important features including the actuators, platforms, and levers are

completed. The backside fabrication starts with depositing the protection material photoresist on the top surface to protect it during the backside etching. After protecting the front side, the lithographically patterning is done on the bottom side and then deep reactive ion etched up to the buried oxide layer (See Figure 7(d)). After the backside etching, the buried oxide layer is etched away with Buffered Oxide Etchant (B.O.E.) to release the moving parts for 2 DOF motion.

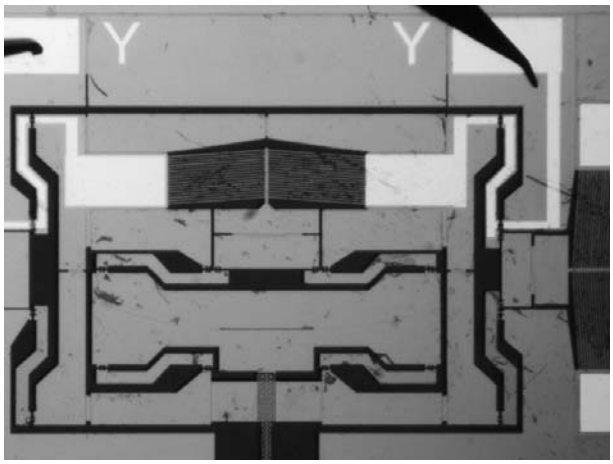

(a) Fabricated inner and outer platforms

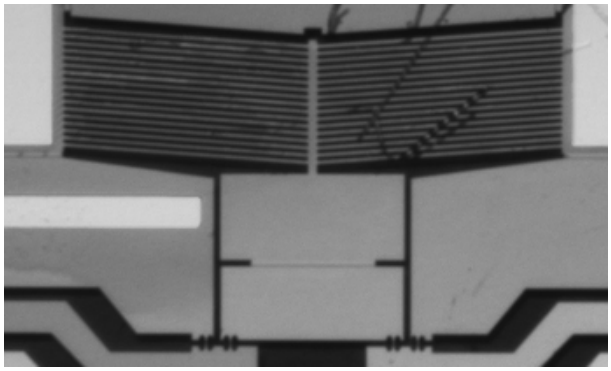

(b) Physical separation between actuator and moving platform for electric isolation

(c) Built-in probe extended from two opposing nanopositioners

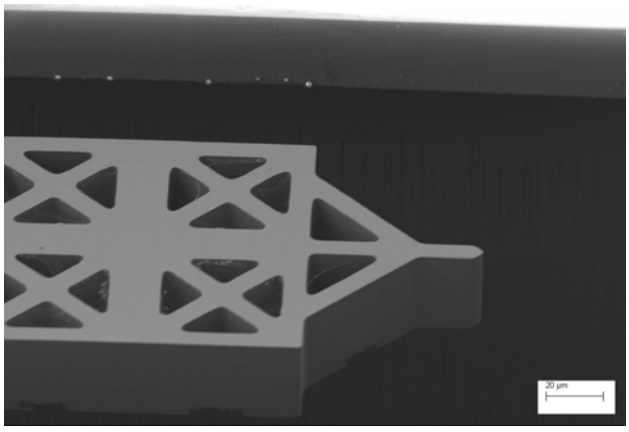

(d) SEM micrograph of the built-in probe tip

Figure 8. Fabricated 2 DOF nanopositioner

Figure 8(a) shows the inner platform fully surrounded by the outer platform in the 2 DOF nanopositioner. The metal pads next to the two letters "Y" are the electric connections for the inner actuation system. The two metal pads and the electrothermal actuator on the right side are the electric connections for the outer platform. The probe tips shown in Figure 8(a) are used for electric connection. The actuator connecting rod trench in the close-up view shown in Figure 8(b) is for electric isolation between the two actuators. The backside supporting layer below the trench is still connected through the silicon dioxide insulation layer to the two parts of the actuator connecting rod and can deliver the force generated by the actuator efficiently. The inner platform built-in probe shown in 8(c) is added to this nanopositioner for possible nano-scale manipulation. The top view and angled view are shown in Figure 8(c) and 8(d). Figure 8(d) is taken in the JEOL SEM [16]. Due to the limited field of view of the SEM [17, 18], the probe tip with the reference features are exploited to measure the displacement of the nanopositioner.

4 EXPERIMENTAL ANALYSIS

In order to demonstrate the performance and usability of the proposed design concept, the fabricated 2 DOF nanopositioners were tested under the Veeco[1] optical profiler. The main objectives of this experiment are 1) to measure the nanopositioner maximum displacement or performance before any electrothermal actuator beam buckling and 2) to measure the cross talk error by the two moving platforms.

The two single DOF platforms are driven by two separate DC power suppliers and all the tests are performed at room temperature. The displacement is calculated by measuring the distance of the built-in probe tip from the two red reference blocks shown in Figure 9(a), located on both sides of the probe tip. The two blocks are fixed reference structures with a width of 150 μm. Based on this relationship, the X, Y, and Z distances are measured from the reference features as shown in Figure 9(b).

The experimental test for the coupling motion of the 2 DOF nanopositioner is to measure the axis motion kept in the same position, while the other axis is in motion. If there is no cross coupled motion, the stationary axis is expected to remain in exactly the same position.

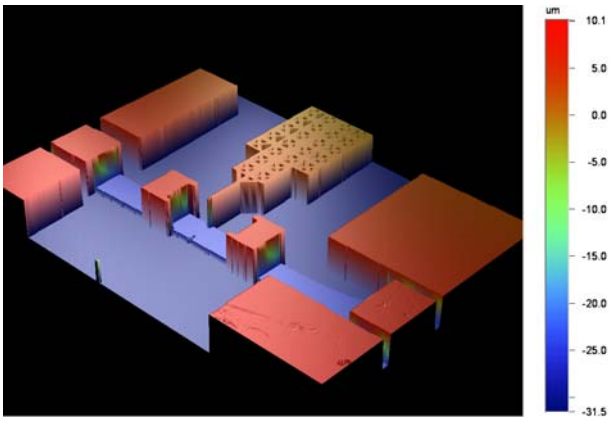

(a) 3D image of built-in tip for displacement measurement

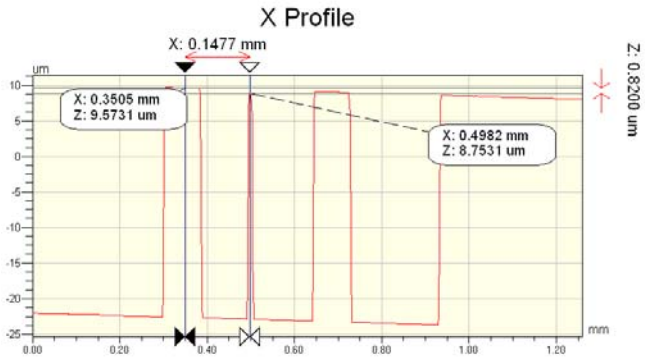

(b) Distance measurement results between built-in probe tip and red block references shown in (a)

Figure 9. Displacement measurements under Veeco[1] Optical profiler

Figure 10 shows coupled motion displacement measurement results from the Veeco optical profiler for two different cases. The coupled motion (cross talk error) and maximum range of motion are tested at the same time by measuring the displacement on two orthogonal axes, when one platform is in motion, while the other is not. The result is shown in Figure 10(a).

The actuated axis can have about 55 μm displacement before buckling occurs. The coupling motion was negligible. The maximum recorded error was ± 1.5 μm which is less than 2.7 % of the maximum displacement and its standard deviation is 0.828 um. Simultaneous 2 DOF motion was also tested and the result is shown in Figure 10(b). When one platform moves to its maximum range, the other platform is actuated to move to a certain position; the line (a) in Figure 10(b) is a motion graph when the inner platform moves from 15 μm to 65 μm displacements, while the outer platform has moved by 13 μm. The line (b) is the motion graph when the outer platform moves from 20 μm to 55 μm, while the inner platform has moved by 20 μm. The line (c) is the trajectory when the inner platform moves from 20 μm to 65 μm, while the outer platform has moved by 55 μm.

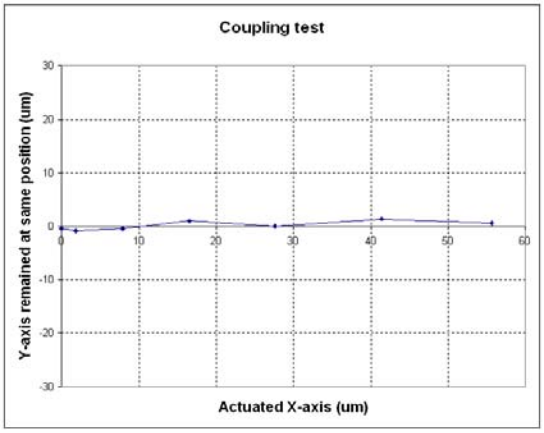

(a) Coupling motion measurement. One actuator is moving the other actuator is not

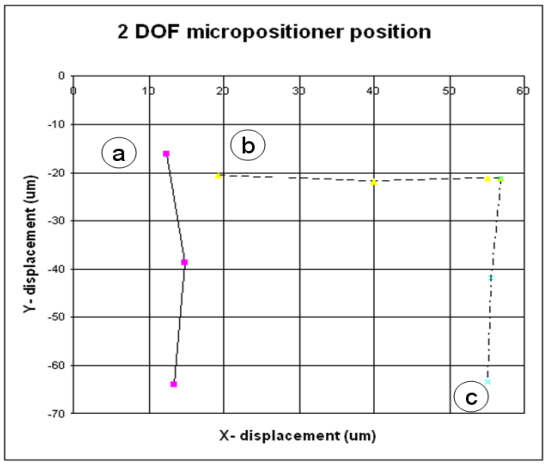

(b) Maximum motion of range in 2 DOF motion

Figure 10. Distance operation in 2 DOF motion

There are three possible sources of error associated with these measurements; 1) displacements measured by the microscope CCD camera imaging system, which has limited resolution and thus it is difficult to track the same target point from one image frame to the next, 2) the plane of the moving platform motion not perfectly orthogonal to the centerline of the microscope imaging system camera resulting in a small cosine error, and 3) the electrothermal actuator drift.

5 CONCLUSIONS

Our nanopositioners are used for high precision testing, metrology, interfaces, and standards work. The objective of our design has been to minimize open loop angular deviation and cross talk errors, while maximizing the range of motion. Because of the novel nested nanopositioner mechanism design, we were very successful in accomplishing those goals for the macro and meso-scale versions of these devices. The first generation of our micro-scale MEMS versions of the nanopositioners that used the double parallelogram design discussed in this paper did not meet those goals.

This paper describes the design, fabrication, and testing of the second generation of our 2 DOF nanopositioner with decoupled XY axes motion and a significant increase in the motion range. This was accomplished by 1) designing a fully nested 2 DOF motion platform with low cross-coupling between its X and Y axes motion, 2) introducing suspended anchors for a fully nested structure, 3) utilizing two levers and four flexures for the electric power connections of the inner platform, and 4) designing the electrothermal actuator considering the external platform mechanical load for a displacement of 50 μm to 60 μm.

The suspended anchors of the electrothermal actuator in the fully nested motion platform play an important role to hold the actuator in position and to generate acceptable displacement. The electric power connection though flexures and levers also proved very useful in order to control the nested released structure, because it is not possible to transfer electric power by conventional wire bonding.

The coupling error was measured. The results showed that it was negligible when using the fully nested nanopositioner design.

We currently use manual (master-slave) real-time vision feedback control to operate our nanopositioners inside a Scanning Electron Microscope (SEM) chamber. A new generation of these devices includes embedded sensors and their design will be reported in a future paper.

6 ACKNOWLEDGEMENT

We would like to thank Dr. Seung Ho Yang and Dr. Jae Myung Yoo for their valuable MEMS advice and encouragement. We would also like to thank Dr. Young-Man Choi for ANSYS FEA advice and support.

REFERENCES

[1] W. P. Sassen, V.A. Henneken, M. Tichem, P. M. Sarro, "An improved in-plane thermal folded V-beam actuator for optical fibre alignment," J. Micromech. Microeng. 18 (2008) 075033.

[2] S. Bergna, J. J. Gorman, N. G. Dagalakis, "Design and Modeling of Thermally actuated MEMS Nanpositioner," Proceedings of IMECE2005, 2005 ASME International Mechanical Engineering Congress and Exposition, Nov. 5-11, 2005, Orlando, Florida USA.

[3] T. C. Du, G. Lau, P. M. Sarro, "Polymer Thermal Microactuator With Embedded Silicon Skeleton: Part II-Fabrication, Characterization, and Application for 2-DOF Microgripper," J. Microelectromechanical systems. Vol 17, No.4, August 2008.

[4] G.F. Christopher, J.M. Yoo, N. Dagalakis, S.D. Hudson, K.B. Migler, "Development of a MEMS based Dynamic Rheometer," The Royal Society of Chemistry Lab on a Chip Journal, 10 (2010), pp 2749-2757.

[5] B. J. Yi, G. B. Chung, H. Y. Na, W. K. Kim, I. H. Suh, "Design and experiment of a 3-DOF parallel micromechanism utilizing flexure hinges", IEEE Transactions on Robotics and Automation, Aug. 2003, Vol. 19, Issue 4, pp 604-612.

[6] H. N. Kwon, S. H. Jeong, S. K. Lee and J. H. Lee "Design and characterization of a micromachined inchworm motor with thermoelastic linkage actuators", Sensors Actuators A 2003, 103. pp 143–9.

[7] H. Guckel, K. Fischer and E. Stiers "Closed loop controlled, large throw, magnetic linear microactuator with 1000 micron structural height", Proc. IEEE Int. Conf. On Micro Electro Mechanical Systems, 1998, pp 414–8.

[8] L. Que, J.S. Park, Y.B. Gianchandani, "Bent-beam electrothermal actuators: Part I. Single beam and cascaded

devices", IEEE/ASME J. Microelectromech. Syst., 10, pp 247–54, 2001.

[9] M.S. Baker, J.A. Walraven, T.J. Headley, "Final Report: Compliant Thermo-mechanical MEMS Actuators, LDRD# 52553", RA Plass 2004 p. 15.

[10] Y. B. Gianchandani and K. Najafi "Bent-beam strain sensors", IEEE J. Microelectromech. Syst., 1996, 5 pp.52–8.

[11] S.T. Smith. "Flexure; Elements of Elastic Mechanism.", Gordon and Breach Science Published, 2000.

[12] R. M. Johnes, “Buckling of Bars, Plates, and Shells”, 2008, pp73-75.

[13] D. Mukhopadhyay, J Dong, E. Pengwang, Ferreira, "A SOI MEMS-based 3-DOF Planar Parallel-Kinematics Nanopositioning Stage", Sensors and Actuators A: Physical, 147(1), 340-351, (2008).

[14] K. Miller, A. Cowen, G. Hames, B. Hardy, "SOIMUMPs Design Handbook" MEMSCAP, revision 4.0 ", http://www.memscap.com/mumps/documents/SOIMUMPs.dr.v4.pdf".

[15] ANSYS Multiphysics version 11 help manual in http://www.ansys.com/Products/Simulation+Technology/Multiphysics/ANSYS+Multiphysics.

[16] JEOL NEoScope Benchtop SEM in http://www.jeolusa.com/PRODUCTS/ElectronOptics/ScanningElectronMicroscopesSEM/PortableandBenchtop/NeoScopeBenchtopSEM/tabid/511/Default.aspx.

[17] DMEMS Dynamic MEMS Measurement Option for Wyko NT1100 Optical Profiler, in http://www2.veeco.com/pdfs.php/396/?showPDF=true.

[18] S.H. Yang, Y.S. Kim, K.P. Purushotham, J.M. Yoo, Y.M. Choi, N. Dagalakis, "AFM characterization of nanopositioner in-plane stiffnesses", Sensors and Actuators A .163 (2010), pp 383–387.

[19] J.J. Gorman, Y.S. Kim, A.E. Vladar, N.G. Dagalakis, “Design of an on-chip microscale nanoassembly system”, International Journal of Nanomanufacturing, Vol. 1, Number 6, 2007, pp710-721.

[20] R. Murthy, D. O. Popa, "WAFER SCALE FACTORIES USING ASSEMBLED MEMS ROBOTS", Proceedings of the ASME 2010 International Design Engineering Technical Conferences & Computers and Information in Engineering Conference, IDETC/CIE 2010, August 15-18, 2010, Montreal, Quebec, Canada.

[21] D.C. Montgomery, "Design and Analysis of Experiments", 5th edition, John wiley & Sons, Inc., 2001, p170-171, p218-219

[22] 10-step analysis software in http://www.itl.nist.gov/div898/education/datasets.htm

[23] J.T. Fong, R. deWit, P.V. Marcal, J.J. Filliben, N.A. Heckert, "A Design-of-Experiments Plug-In for Estimating Uncertainties in Finite Element Simulations", 2009 SIMULIA Customer Conference, May 18-21, 2009, London, U.K.